CrossMark

Template-free hydrothermal synthesis and luminescence properties of NaGd(WO$_4$)$_2$:Eu^{3+} red phosphors with controlled morphology

Yongqing Zhai[1] · Xin Zhao[1] · Qinglin Sun[1] · Shuai Yang[1] · Derui Deng[1] · Yaru Liu[1] · Manhong Miao[1] · Jing Wang[1]

Abstract

A series of morphology-controlled NaGd(WO$_4$)$_2$:Eu^{3+} phosphors were prepared by a facile hydrothermal method in the absence of any surfactants and templates. X-ray diffraction, scanning electron microscopy and photoluminescence spectra were used to characterize the obtained products. It was found that the pH value of the precursor solution had a remarkable impact on the phase structure, morphology and luminescent properties of the products. The possible formation mechanism for square plate structure was proposed based on the time-dependent experiments. Moreover, the effects of the initial pH value, reaction time and Eu^{3+} concentration on the luminescent properties of NaGd(WO$_4$)$_2$:Eu^{3+} phosphors were investigated in detail. The results revealed that the square plate-like microcrystals synthesized at pH = 8 for 20 h showed excellent red emission under near-ultraviolet (NUV) excitation. In addition, no concentration quenching occurred when the Eu^{3+} concentration was as high as 0.6. The intense red emission and high red color purity showed that NaGd(WO$_4$)$_2$:Eu^{3+} microplates had promising applications as red component in NUV-excited WLEDs.

1 Introduction

Undoubtedly, chemical and physical properties of inorganic materials are greatly affected by their crystal structure, phase, size and shape [1–4]. So a broad attention has been paid on the synthesis of inorganic nano/micromaterials with special size and well-defined morphology, which are potentially applied in various fields such as photochemistry, optoelectronics, solar cells, color displays, catalysis, ceramics, advanced materials, etc [5, 6].

In recent years, as a kind of important inorganic functional materials, rare earth doped luminescent nano/micromaterials have become a research hotspot due to their attractive optical properties. Among them, rare earth ions doped double tungstate phosphors have attracted great interest because of their unique structure, excellent physical and chemical stability, promising luminescence properties and potential applications in display and lighting [7, 8]. Nowadays, there have been some reports on the morphology

controlled synthesis of tungstate luminescent materials. Wang et al. prepared NaLu(WO$_4$)$_2$:Eu^{3+} microcrystals with tunable morphology from hexahedron to tetrahedron via an EDTA-aided hydrothermal process [9]. Yang et al. reported the preparation of spindle and hierarchical petaloid NaGd(WO$_4$)$_2$:Eu^{3+} microcrystals through hydrothermal route using PVP and Na$_3$Cit as surfactants [10]. Liu et al. reported the synthesis of NaLa(WO$_4$)$_2$ microspindles, microplates, microdumbbells and paired microspheres via hydrothermal method with the addition of EDTA-2Na [11]. Wang et al. synthesized zero-dimensional ellipsoid-like and one-dimensional rod-like NaGd(WO$_4$)$_2$:Eu^{3+} microcrystals by the microemulsion mediated hydrothermal method [12]. Generally, the hydrothermal method is used to synthesize the products with uniform size and defined morphology due to its simple preparation process, low reaction temperature, and mild reaction conditions [13, 14]. However, the addition of templates and surfactants which may have toxicity will increase costs and introduce impurities in the products [15]. Therefore, it remains challenging to develop a low-cost and environment-friendly method for the synthesis of nano/microcrystals with different morphologies.

As the fourth generation solid-state light sources, white light emitting diodes (WLEDs) have received considerable attention. An efficient approach to fabricate WLEDs with high color rendering index and suitable correlated color

✉ Yongqing Zhai
zhaiyongqinghbu@163.com

✉ Jing Wang
wangjing9804@163.com

[1] College of Chemistry and Environmental Science, Hebei University, Baoding 071002, China

temperature is to combine near-ultraviolet LED chip with the tricolor phosphors [16]. However, the commercial red phosphors have unstable chemical properties and unsatisfied luminous efficiency compared with blue and green phosphors [17]. Therefore, it is of great importance to develop stable red phosphors which have effective absorption in near-UV (NUV) region. Among all the rare earth ions, Eu^{3+} is considered as the promising activator for red emitting due to its $^5D_0 \rightarrow {}^7F_J$ transitions which have excellent red color purity [18].

In this paper, NUV-excited $NaGd(WO_4)_2$:Eu^{3+} red phosphors with various morphologies were synthesized by a facile hydrothermal method without any templates and surfactants. The effects of the starting pH value and reaction time on the phase composition, morphology and luminescent properties of the products were discussed. In addition, the possible formation mechanism for square plate-like microcrystals with excellent luminous performance was proposed. Finally, the concentration of luminescent center Eu^{3+} as a key factor to the luminescent property of $NaGd(WO_4)_2$:Eu^{3+} phosphors was investigated.

2 Experimental

2.1 Materials

$Na_2WO_4 \cdot 2H_2O$ (A.R.), Gd_2O_3 (99.99%), Eu_2O_3 (99.99%), NaOH (A.R.) and HNO_3 (A.R.) were used as starting materials without any further purification. $Gd(NO_3)_3$ (0.3990 M) and $Eu(NO_3)_3$ (0.0967 M) solutions were prepared by dissolving a certain amount of Gd_2O_3 and Eu_2O_3 in dilute nitric acid under magnetic stirring and water bath heating.

2.2 Synthesis

For the synthesis of $NaGd_{0.95}(WO_4)_2$:$0.05Eu^{3+}$ phosphor, 7.04 mL 0.3990 M $Gd(NO_3)_3$ and 1.53 mL 0.0967 M $Eu(NO_3)_3$ solutions were mixed into 40 mL deionized water firstly. Then, 20 mL sodium tungstate solution containing 8.88 mmol $Na_2WO_4 \cdot 2H_2O$ was dropwise added into the above mixture under vigorous stirring to form milky colloidal suspension. The pH value of the reaction system was adjusted respectively to 6, 7, 8, 9 by dropping HNO_3 (2 M) or NaOH (2 M) solution. After continuous stirring for 30 min, the white precipitate was transferred to a 100 mL Teflon-lined stainless steel autoclave, and then heated at 180 °C for 20 h. Finally, when the autoclave was naturally cooled down to room temperature, the products were centrifuged, washed with deionized water and ethanol for several times, and then dried at 50 °C for 10 h.

2.3 Characterization

The crystal structure and phase purity of the samples were examined by X-ray diffraction (XRD) performed on a Brucker D8-advance diffractometer with Cu Ka radiation (40 kV × 40 mA, $\lambda = 0.15406$ nm) in the 2θ range from 15° to 65°. The morphology and elemental composition of the samples were characterized by a Phenom ProX scanning electron microscope (SEM) equipped with an energy-dispersive X-ray spectrum (EDS). The photoluminescence (PL) excitation and emission spectra were recorded with F-380 fluorescence spectrophotometer using a 450 W Xe lamp as the excitation source. The CIE chromaticity coordinates and color purity of samples were recorded on a HP-8000 fast spectrophotocolorimeter. All the measurements were performed at room temperature.

3 Results and discussion

3.1 Phase identification and morphology

Figure 1 shows the XRD patterns of the samples synthesized under different pH values for 20 h at 180 °C. It can be clearly found that pH value has a significant effect on phase structure and purity. When the pH value is 6, the impurity peaks of WO_3, Gd_2O_3 and $Gd_2(WO_4)_3$ can be observed. Whereas the pH value is adjusted to 7 or 8, no traces of impurity phases appears and all of the diffraction peaks are matched to the standard card of $NaGd(WO_4)_2$ (JCPDS No. 25-0829) with space group of $I4_1/a$ (88). Moreover, the diffraction peaks become sharp and strong, indicating that tetragonal pure phase $NaGd(WO_4)_2$ with good crystallinity can be obtained under above pH value. This can be further verified
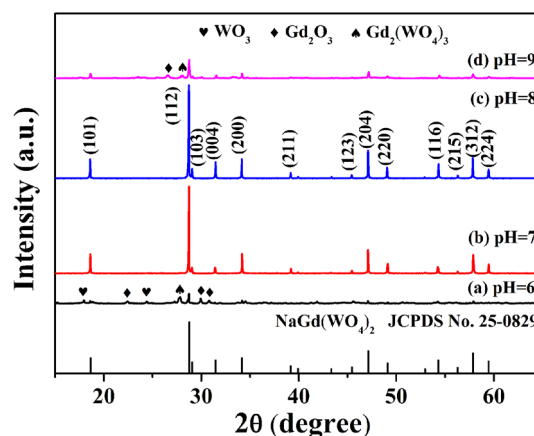

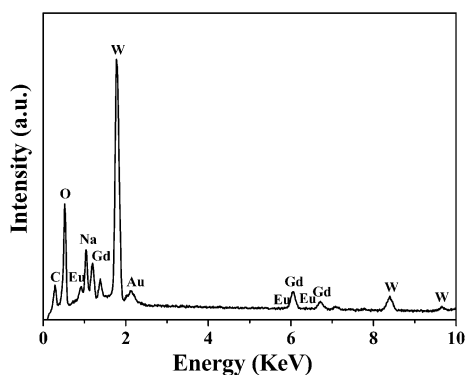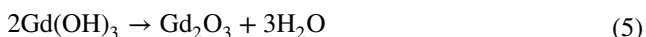**Fig. 1** XRD patterns of the samples prepared at different pH values for 20 h at 180 °C

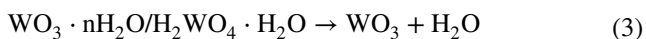**Fig. 2** EDS pattern of $NaGd_{0.95}(WO_4)_2{:}0.05Eu^{3+}$ phosphor

by EDS pattern of $NaGd_{0.95}(WO_4)_2{:}0.05Eu^{3+}$ phosphor obtained at pH = 8, as shown in Fig. 2. It is clear that the product contains Na, Gd, Eu, W and O elements. However, further increasing the pH value to 9, the intensity of the diffraction peak is obviously weakened and impurity phases of Gd_2O_3 and $Gd_2(WO_4)_3$ can be detected.

The effect of pH value on phase structure can be explained as follows. When Na_2WO_4 solution is added into $Gd(NO_3)_3$ and $Eu(NO_3)_3$ mixed solution, a part of WO_4^{2-} ions combine with Gd^{3+} to form indissolvable $Gd_2(WO_4)_3$. In acidic reaction system (pH = 6), some WO_4^{2-} ions react with H^+ to produce $WO_3{\cdot}nH_2O$ or $H_2WO_4{\cdot}H_2O$ [12]. Then $WO_3{\cdot}nH_2O$ or $H_2WO_4{\cdot}H_2O$ dehydrates and forms WO_3 under hydrothermal conditions with high temperature and pressure environments. In addition, under hydrothermal conditions, a portion of Gd^{3+} ions are hydrolyzed to $Gd(OH)_3$ and release H^+, which promotes the reaction of WO_4^{2-} and H^+. Meanwhile, the generated $Gd(OH)_3$ dehydrates and transforms into Gd_2O_3. The involved reactions maybe:

$$3WO_4^{2-} + 2Gd^{3+} \rightarrow Gd_2(WO_4)_3 \tag{1}$$

$$WO_4^{2-} + H^+ \rightarrow WO_3 \cdot nH_2O/H_2WO_4 \cdot H_2O \tag{2}$$

$$WO_3 \cdot nH_2O/H_2WO_4 \cdot H_2O \rightarrow WO_3 + H_2O \tag{3}$$

$$Gd^{3+} + 3H_2O \rightarrow Gd(OH)_3 + 3H^+ \tag{4}$$

$$2Gd(OH)_3 \rightarrow Gd_2O_3 + 3H_2O \tag{5}$$
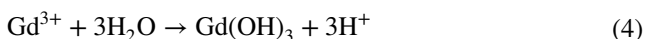
Under alkaline condition (pH = 9), Gd^{3+} ions can not only combine with WO_4^{2-} to form $Gd_2(WO_4)_3$, but also tend to react with OH^- to form $Gd(OH)_3$. Then $Gd(OH)_3$ decomposes into Gd_2O_3 under hydrothermal conditions. The relevant chemical reaction equations are given as follows:

$$2Gd^{3+} + 3WO_4^{2-} \rightarrow Gd_2(WO_4)_3 \tag{6}$$

$$Gd^{3+} + 3OH^- \rightarrow Gd(OH)_3 \tag{7}$$

$$2Gd(OH)_3 \rightarrow Gd_2O_3 + 3H_2O \tag{8}$$
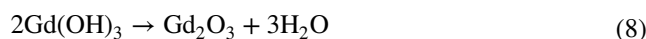
The SEM images of the samples prepared at different pH values are displayed in Fig. 3. It is obvious that the samples with different morphology can be formed by adjusting the pH value of the solution. When pH = 6, the sample is composed of microspheres with the average diameter of 3 μm. It can also be seen that the surface of the microsphere is attached by a large number of small nanoparticles. As the pH value is enhanced to 7, the morphology of the sample becomes shuttle-like tetrahedrons, which have four smooth and curved surfaces. When the pH value is further increased to 8, well-dispersed and uniform square plate-like microcrystals can be obtained. The sizes of the microplates are about 4.5 μm in side length and 2.5 μm in center thickness. At the pH value of 9, it can be observed that square microplates disappear and the sample exhibits irregular sheet-like morphology.

From the above experimental results, it can be found that the pH value of reaction system plays a significant role in the formation of pure phase and regular morphology of $NaGd(WO_4)_2$ microcrystals. Because $NaGd(WO_4)_2$ belongs to tetragonal system, the surface energy of {001} planes is higher than {101} planes [15], which results in the faster growth along the [001] direction. As a consequence, the {001} planes will disappear and not be expressed in the final equilibrium morphology, which leads to the formation of shuttle-like tetrahedrons (pH = 7) enclosed by exposed {101} planes. When pH value is increased to 8, excessive WO_4^{2-} will preferentially absorb
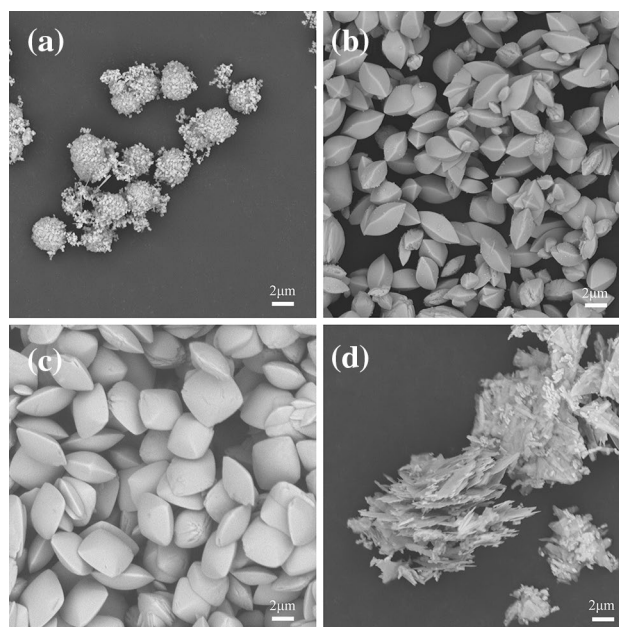

Fig. 3 SEM images of the samples synthesized at 180 °C for 20 h at **a** pH = 6, **b** pH = 7, **c** pH = 8, **d** pH = 9

on {001} crystal planes which have a higher packing density of Na^+ and Gd^{3+} ions than other planes, thus reducing the surface energy and reactivity of {001} planes, then inhibiting their growth [19, 20]. As a result of the minimization of total surface energy, square plates microcrystals can be formed. However, lower or higher pH value (pH = 6 or 9) will change the growth rate of crystal planes with different surface energies. Consequently, the nucleation and growth behavior will be out of kinetic control and the final products tend to be irregular and impure [21].
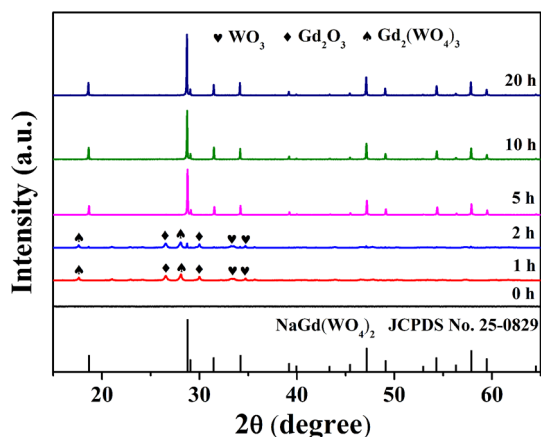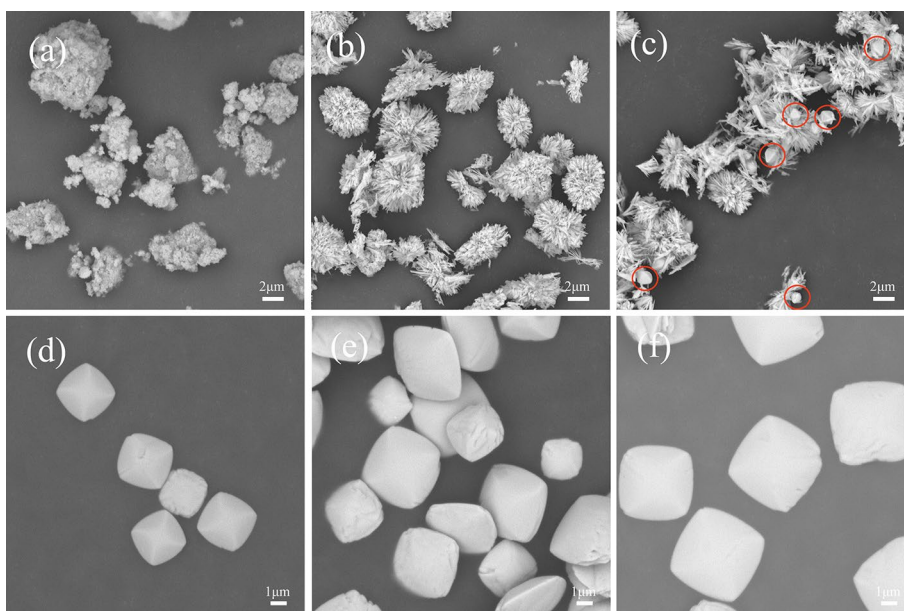

Fig. 4 XRD patterns of the samples synthesized at 180 °C and pH = 8 with different reaction times

3.2 Possible formation mechanism of square plate-like NaGd(WO₄)₂:Eu³⁺ microcrystals

In order to explore the growth process of the microplate, a series of time-dependent experiments were performed. The formation mechanism can be revealed from the crystal structures and morphologies of the samples synthesized at different reaction stages. The corresponding XRD patterns and SEM images are presented in Figs. 4 and 5. It can be seen from Fig. 4 that the product without hydrothermal treatment is amorphous. When the hydrothermal reaction time is 1 or 2 h, the weak diffraction peaks of the intermediates WO_3, Gd_2O_3 and $Gd_2(WO_4)_3$ can be observed. Meanwhile, the phase of $NaGd(WO_4)_2$ (JCPDS No. 25-0829) emerges at the hydrothermal time of 2 h. As the reaction is prolonged to 5 h, the peaks of impurities have disappeared completely and those of $NaGd(WO_4)_2$ become strong, indicating that the pure tetragonal phase $NaGd(WO_4)_2$ has been formed. With the reaction proceeding to 10 and 20 h, the intensity of the peaks is enhanced, which suggests that the crystallinity of samples is improved.

Figure 5 presents the SEM images of samples synthesized at different reaction stages. As shown in Fig. 5a, after adjusting pH value to 8 before hydrothermal treatment, the sample is composed of irregular and flocculent particles assembled by numerous tiny particles. After hydrothermal reaction for 1 h (Fig. 5b), the flocculent particles evolve to dandelion-like microspheres with numbers of microneedles spreading from center. When the hydrothermal reaction time is prolonged to 2 h (Fig. 5c), the microspheres disintegrate into irregular needle clusters, and a small amount of primary $NaGd(WO_4)_2$ microcrystals appear (marked with circles in Fig. 5c). As further proceeding to 5 h (Fig. 5d),

Fig. 5 SEM images of the microcrystals obtained at 180 °C and pH = 8 under different hydrothermal reaction time **a** 0 h, **b** 1 h, **c** 2 h, **d** 5 h, **e** 10 h and **f** 20 h. (Color figure online)

the microneedles disappear completely and transform into square plate-like $NaGd(WO_4)_2$ microcrystals with the size of about 3 μm. With increasing the hydrothermal reaction time to 10 h (Fig. 5e), the microplates grow gradually, but the size distribution is nonuniform. When the time is extended to 20 h (Fig. 5f), the perfect and uniformed square plates are obtained, and the size of microplates is increased to about 4.5 μm. It is thus demonstrated that crystal growth is a complicated phase transition process and needs a moderate ripe time.

It is commonly known that the morphological evolution is influenced by thermodynamics and kinetics. The grain size depends on the nucleation and growth rate of the crystal from the kinetic mechanism of crystal formation. The crystallization process tends to proceed along the direction in which the surface free energy is reduced [22]. When the Na_2WO_4 is added into the rare earth nitrate mixture, the white precipitates with high surface energy appear as precursors. In the hydrothermal process, the precursors are converted into aggregated microneedles, and further assembled into dandelion-like microspheres so as to reduce the free energy from the viewpoint of thermodynamics. Then microneedles dissolve and recrystallize to form primary crystals, followed by growth. Finally, the large particles grow up at the cost of small ones in order to further reducing surface energy. From the above analysis, it can be deduced that the formation of square plate-like $NaGd(WO_4)_2$ crystal may be ascribed to the nucleation–dissolution–recrystallization–further growth mechanism.

3.3 Luminescence properties

The excitation and emission spectra of $NaGd_{0.95}(WO_4)_2$:0.05Eu^{3+} are shown in Fig. 6. It can be seen that the excitation spectrum monitoring the emission at 614 nm consists of two parts: one is a broad excitation band from 230 to 350 nm with a maximum at 269 nm, which is caused by W–O and Eu–O charge transfer transitions [23]; the other part is composed of a series of narrow excitation peaks in the range of 350–500 nm, belonging to the $^7F_0 \rightarrow {}^5D_4$ (362 nm), $^7F_0 \rightarrow {}^5L_7$ (381 nm), $^7F_0 \rightarrow {}^5L_6$ (394 nm), $^7F_0 \rightarrow {}^5D_3$ (416 nm) and $^7F_0 \rightarrow {}^5D_2$ (465 nm) electron transitions of Eu^{3+}, respectively [23]. Among these excitation peaks, the strongest peak is located at 394 nm. Therefore, $NaGd(WO_4)_2$:Eu^{3+} phosphors can be effectively excited by NUV (380–410 nm) LED chips.

Under the excitation of 394 nm, $NaGd_{0.95}(WO_4)_2$:0.05Eu^{3+} phosphor exhibits a series of linear characteristic emission peaks located at 592, 614, 654 and 701 nm, which are ascribed to transitions from the excited state $^5D_0$ to ^7F_J ($J = 1, 2, 3, 4$) levels of Eu^{3+}, respectively. Generally, the $^5D_0 \rightarrow {}^7F_1$ magnetic dipole transition is hardly affected by the crystal field around Eu^{3+} ions, which is dominant when
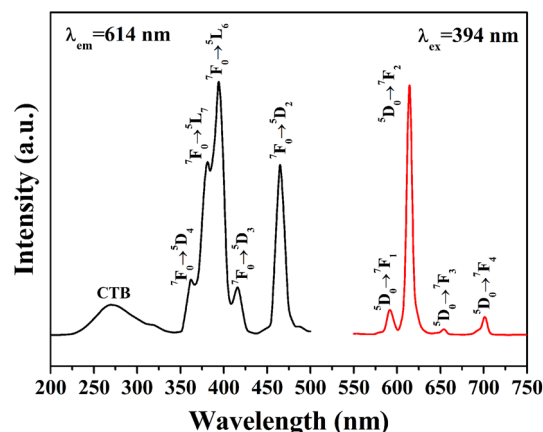

Fig. 6 The excitation and emission spectra of $NaGd_{0.95}(WO_4)_2$:0.05Eu^{3+} phosphor prepared at pH = 8 and 180 °C for 20 h
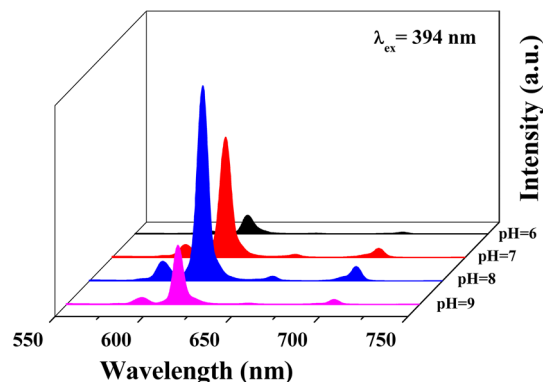

Fig. 7 The emission spectra of the phosphors obtained at 180 °C for 20 h at various pH values

the Eu^{3+} ions are in the symmetrical center lattice. However, $^5D_0 \rightarrow {}^7F_2$ electric dipole transition is a highly sensitive transition which is strongly influenced by the chemical environment surrounding the luminescent center. When the Eu^{3+} ions occupy the low symmetry sites without an inversion center, the $^5D_0 \rightarrow {}^7F_2$ transition is primary [24]. Obviously, for as-synthesized sample, the emission intensity of 614 nm is much higher than that of 592 nm, which strongly demonstrates that Eu^{3+} ions mainly occupy the asymmetric sites in the $NaGd(WO_4)_2$ matrix and the prepared phosphors possess high red color purity.

The emission spectra of the phosphors obtained at different pH value are given in Fig. 7. It can be observed that the shape and location of the emission spectra are less affected by pH value, but the intensity depends strongly on pH value. As shown in Fig. 3, the samples prepared under different pH value have various morphologies, indicating that the luminous characteristics are related to the morphology of the samples. With the change of pH value from 6 to 9, the red

emission intensity increases gradually, and then decreases dramatically. The phosphor synthesized at pH = 8 has the strongest emission intensity.

The reasons for above result may be as follows. When the pH value is 6 or 9, the sample has low phase purity and crystallinity (shown in Fig. 1), thus exhibits the weak luminous intensity. At the pH value of 7 or 8, the as-synthesized sample is pure $NaGd(WO_4)_2$:Eu^{3+} with high crystallinity, so the emission intensity is remarkably improved. In comparison, the luminescent intensity of the sample with square plate morphology (pH = 8) is higher than that with the morphology of shuttle-like tetrahedron (pH = 7). This is because the electronic structures can be altered due to the changes in the morphology of the samples, which affects the transition of the luminescent center from the ground state to the excited state and the release of photons from the sample surfaces [25]. Therefore, it can be deduced that square plate morphology is more conducive to the emission in the red region, which demonstrate the viewpoint that morphology control is of great importance for improving the luminescence performance of samples [26, 27].

Figure 8 shows the emission spectra of the phosphors prepared under various reaction times at pH = 8. It is obvious that the red emission intensity gradually increases with extending the hydrothermal reaction time. From 0 to 5 h, the increasing rate of the luminous intensity is relatively fast, but after 5 h of reaction, the rate becomes slow. This result is matched well with those of XRD and SEM analysis shown in Figs. 4 and 5. When the hydrothermal reaction time is 5 h, the impurities have disappeared completely and pure tetragonal phase $NaGd(WO_4)_2$ has been formed. In addition, the morphology becomes uniform and perfect. High crystallinity and uniform morphology tend to reduce the surface recombination rate, which means the less nonradiative decay losses of the surface activator [28, 29], so the luminescent intensity is imp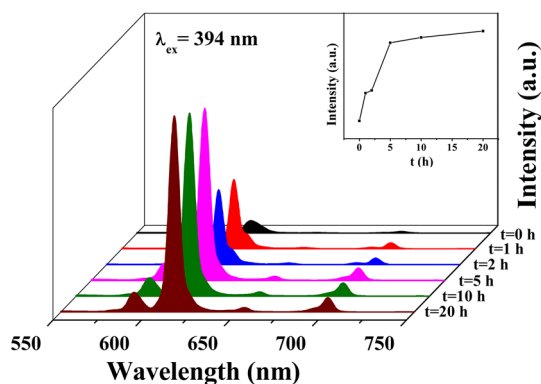roved significantly. Further prolonging the reaction time from 5 to 20 h, the crystallinity and particle size are increased slowly, hence, the emission intensity is enhanced gently.

The concentration of activator also plays a significant role in the luminous intensity. The emission spectra of $NaGd_{1-x}(WO_4)_2$:xEu^{3+} (x = 0.05, 0.1, 0.2, 0.3, 0.4, 0.5, 0.6) phosphors under 394 nm excitation are presented in Fig. 9. We can observe that the emission intensity of the products is gradually enhanced with the increase of Eu^{3+} doping concentration. An interesting finding is that the concentration quenching phenomenon has not yet occurred when the doping concentration (x) of Eu^{3+} ions is as high as 0.6. This is closely related to the scheelite structure of the matrix. In $NaGd(WO_4)_2$ host lattice, W^{6+} is located in the center of the tetrahedron formed by four oxygen atoms, and the Na^+ and Gd^{3+} ions are surrounded by eight oxygen atoms [30]. The doped Eu^{3+} ions are expected to occupy the Gd^{3+} cation sites and the bond angles of Eu–O–W and O–W–O are larger than 100°, leading to a longer distance between Eu^{3+} ions [31]. Thus the resonance energy transfer between Eu^{3+} ions will be inhibited and the quenching concentration of Eu^{3+} ions is high in $NaGd(WO_4)_2$:Eu^{3+} phosphors [32]. The phosphors with higher Eu^{3+} concentration will exhibit strong red emission and can be potentially applied as red phosphors for NUV-excited WLEDs.

In general, the luminous color is crucial for the practical application of phosphors. Figure 10 shows the CIE chromaticity diagram of representative $NaGd_{1-x}(WO_4)_2$:xEu^{3+} (x = 0.05, 0.6) samples under 254 nm excitation and the inset presents the digital image of $NaGd_{0.4}(WO_4)_2$:$0.6Eu^{3+}$ phosphor. The CIE coordinates and color purity of as-prepared $NaGd_{1-x}(WO_4)_2$:xEu^{3+} phosphors with different Eu^{3+} concentration are summarized in Table 1. It can be found that all the color coordinates are close to the standard red CIE coordinates (0.67, 0.33). Moreover, the as-synthesized phosphors show high color purity, which are above 99% when the
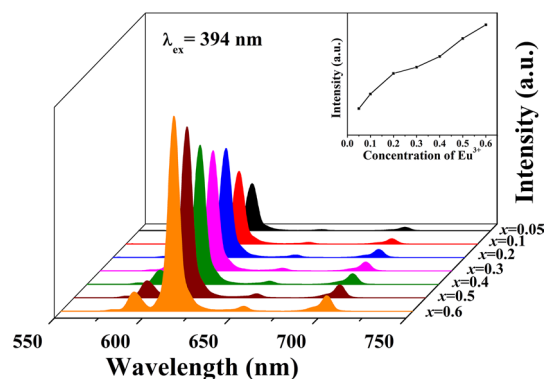

Fig. 8 The emission spectra of the samples prepared at pH = 8 and 180 °C with different reaction times. The inset shows the dependence of emission intensity at 614 nm on the reaction time

Fig. 9 The emission spectra of $NaGd_{1-x}(WO_4)_2$:xEu^{3+} phosphors with different doping concentration of Eu^{3+} synthesized at pH = 8, 180 °C and 20 h. The inset shows the variation trend of emission intensity at 614 nm with Eu^{3+} concentration
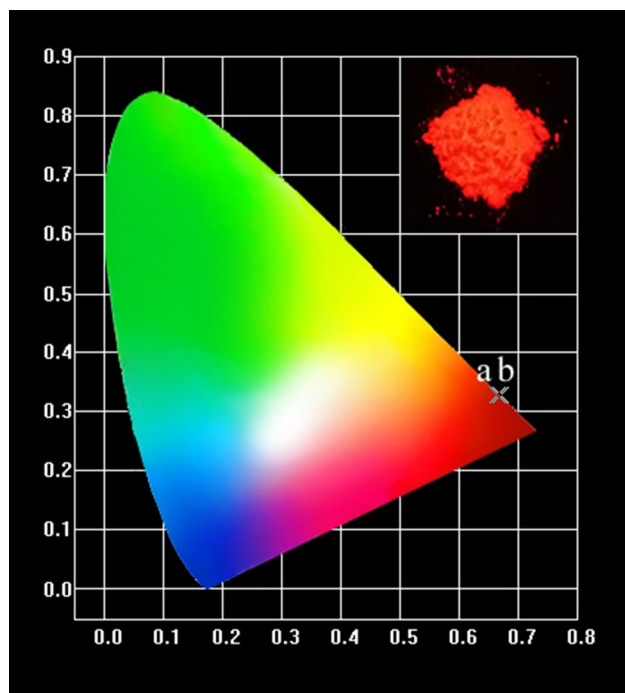
Fig. 10 CIE chromaticity diagram of $NaGd_{1-x}(WO_4)_2$:xEu^{3+} (a: $x = 0.05$; b: $x = 0.6$) phosphors under 254 nm excitation and the digital photograph of $NaGd_{0.4}(WO_4)_2$:0.6Eu^{3+} excited under 254 nm UV lamp

Table 1 CIE chromaticity coordinates and color purity of $NaGd_{1-x}(WO_4)_2$:xEu^{3+} ($x = 0.05$, 0.1, 0.2, 0.3, 0.4, 0.5, 0.6) phosphors

Sample	CIE coordinates		Color purity (%)
	x	y	
$NaGd_{0.95}(WO_4)_2$:0.05Eu^{3+}	0.6642	0.3270	97.4
$NaGd_{0.9}(WO_4)_2$:0.1Eu^{3+}	0.6716	0.3250	99.0
$NaGd_{0.8}(WO_4)_2$:0.2Eu^{3+}	0.6708	0.3260	99.3
$NaGd_{0.7}(WO_4)_2$:0.3Eu^{3+}	0.6720	0.3273	99.5
$NaGd_{0.6}(WO_4)_2$:0.4Eu^{3+}	0.6702	0.3262	99.2
$NaGd_{0.5}(WO_4)_2$:0.5Eu^{3+}	0.6724	0.3273	99.6
$NaGd_{0.4}(WO_4)_2$:0.6Eu^{3+}	0.6700	0.3273	99.9

concentration of Eu^{3+} is in the range of 0.1–0.6. The bright red emission can be observed from the inset of Fig. 10, which demonstrates that $NaGd(WO_4)_2$:Eu^{3+} phosphors may have widespread applications in display and lighting fields.

4 Conclusion

Eu^{3+}-doped $NaGd(WO_4)_2$ phosphors with controllable morphology have been synthesized by a simple hydrothermal method without any additives. The samples obtained at the pH value of 7 or 8 are pure tetragonal phase, which exhibit shuttle-like tetrahedrons and square plates morphology, respectively. Time-dependent experiments reveal the formation process of the square plate-like microcrystal, which is dominated by the nucleation–dissolution–recrystallization–further growth mechanism. Upon NUV excitation, the synthesized phosphors show characteristic red emission ascribed to the $^5D_0 \rightarrow {}^7F_2$ transition of Eu^{3+}. The luminous intensity of the square plate-like sample prepared at the pH value of 8 is stronger than others. The emission intensity of the phosphors is gradually increased with increasing Eu^{3+} concentration. Interestingly, no concentration quenching can be observed within the concentration range of 0.05–0.6. Therefore, well-crystallized and uniform square plate-like $NaGd(WO_4)_2$:Eu^{3+} microcrystals with excellent luminescent properties and high red color purity may be applied as candidates of red phosphors in the field of NUV-excited WLEDs.

Compliance with ethical standards

Conflict of interest The authors declare that they have no conflict of interest.

References

1. B. Zhang, H. Zou, Y. Dai, Y. Song, K. Zheng, X. Zhou, Y. Sheng, Controlled synthesis and morphology dependent luminescence of Lu$_2$O$_2$S:Eu^{3+} phosphors. RSC Adv. **6**, 7846–7853 (2016)
2. K. Zhou, Y. Li, Catalysis based on nanocrystals with well-defined facets. Angew. Chem. Int. Ed. **51**, 602–613 (2012)
3. J. Li, Z. Wu, X. Sun, X. Zhang, R. Dai, J. Zuo, Z. Zhao, Controlled hydrothermal synthesis and luminescent properties of Y$_2$WO$_6$:Eu^{3+} nanophosphors for light-emitting diodes. J. Mater. Sci. **52**, 3110–3123 (2016)
4. S.R. Challa, A.T. Delariva, T.W. Hansen, S. Helveg, J. Sehested, P.L. Hansen, F. Garzon, A.K. Datye, Relating rates of catalyst sintering to the disappearance of individual nanoparticles during Ostwald ripening. J. Am. Chem. Soc. **133**, 20672–20675 (2011)
5. Z. Fu, W. Xia, Q. Li, X. Cui, W. Li, Highly uniform NaLa(MoO$_4$)$_2$:Ln^{3+} (Ln = Eu, Dy) microspheres: template-free hydrothermal synthesis, growing mechanism, and luminescent properties. CrystEngComm **14**, 4618–4624 (2012)
6. J. Zhang, N. Zhang, L. Zou, S. Gan, Formation mechanism and optical properties of CdMoO$_4$ and CdMoO$_4$:Ln^{3+}(Ln = Pr, Sm, Eu, Dy, Ho and Er) microspheres synthesized via a facile sonochemical route. RSC Adv. **4**, 38455–38465 (2014)
7. K.K. Rasu, D. Balaji, S.M. Babu, Spectroscopic properties of Eu^{3+}:KLa(WO$_4$)$_2$ novel red phosphors. J. Lumin. **170**, 547–555 (2016)
8. Y. Zhang, W.T. Gong, J.J. Yu, Z.Y. Cheng, G.L. Ning, Multicolor luminescence properties and energy transfer behaviour in host-sensitized CaWO$_4$:Tb^{3+}, Eu^{3+} phosphors. RSC Adv. **6**, 30886–30894 (2016)

9. Z. Wang, J. Zhong, H. Jiang, J. Wang, H. Liang, Controllable synthesis of $NaLu(WO_4)_2$:Eu^{3+} microcrystal and luminescence properties for LEDs. Cryst. Growth Des. **14**, 3767–3773 (2014)

10. X. Yang, H. Tang, Z. Guo, Morphology-controlled synthesis of $NaGd(WO_4)_2$:Eu^{3+} microcrystals by hydrothermal process. Superlattices Microstruct. **80**, 188–195 (2015)

11. X. Liu, W. Hou, X. Yang, J. Liang, Morphology controllable synthesis of $NaLa(WO_4)_2$: the morphology dependent photoluminescent properties and single-phased white light emission of $NaLa(WO_4)_2$:Eu^{3+}/Tb^{3+}/Tm^{3+}. CrystEngComm **16**, 1268–1276 (2014)

12. Y. Wang, J. Tang, X. Huang, L. Jiang, Luminescence properties of Eu^{3+}:$NaGd(WO_4)_2$ nanoparticles and nanorods. J. Rare Earth **34**, 118–124 (2016)

13. S. Huang, D. Wang, C. Li, L. Wang, X. Zhang, Y. Wan, P. Yang, Controllable synthesis, morphology evolution and luminescence properties of $NaLa(WO_4)_2$ microcrystals. CrystEngComm **14**, 2235–2244 (2012)

14. G. Li, L. Li, M. Li, W. Bao, Y. Song, S. Gan, H. Zou, X. Xu, Hydrothermal synthesis and luminescent properties of $NaLa(MoO_4)_2$:Eu^{3+},Tb^{3+} phosphors. J. Alloys Compd. **550**, 1–8 (2013)

15. A. Li, D. Xu, H. Lin, S. Yang, Y. Shao, Y. Zhang, Z. Chen, Facile morphology-controllable hydrothermal synthesis and color tunable luminescence properties of $NaGd(MoO_4)_2$:Eu^{3+},Tb^{3+} microcrystals. RSC Adv. **5**, 45693–45702 (2015)

16. F. Mo, L. Zhou, Q. Pang, F. Gong, Z. Liang, Potential red-emitting $NaGd(MO_4)_2$:R (M = W, Mo, R = Eu^{3+}, Sm^{3+}, Bi^{3+}) phosphors for white light emitting diodes applications. Ceram. Int. **38**, 6289–6294 (2012)

17. L. Li, L. Liu, W. Zi, H. Yu, S. Gan, G. Ji, H. Zou, X. Xu, Synthesis and luminescent properties of high brightness $MLa(WO_4)_2$:Eu^{3+} (M = Li, Na, K) and $NaRE(WO_4)_2$:Eu^{3+} (RE = Gd, Y, Lu) red phosphors. J. Lumin. **143**, 14–20 (2013)

18. X. Feng, W. Feng, M. Xia, K. Wang, H. Liu, D. Deng, X. Qin, W. Yao, W. Zhu, Co-precipitation synthesis, photoluminescence properties and theoretical calculations of $MgWO_4$:Eu^{3+} phosphors. RSC Adv. **6**, 14826–14831 (2016)

19. Y. Zhai, W. Zhang, Y. Yin, Y. Han, X. Zhao, H. Ding, N. Li, Morphology tunable synthesis and luminescence property of $NaGd(MoO_4)_2$:Sm^{3+} microcrystals. Ceram. Int. **43**, 841–846 (2017)

20. S. Liu, D. Yang, D. Ma, S. Wang, T. Tang, S. Huang, Single-crystal $NaY(MoO_4)_2$ thin plates with dominant {001} facets for efficient photocatalytic degradation of dyes under visible light irradiation. Chem. Commun. **47**, 8013–8015 (2011)

21. X. Sun, Y. Li, Size-controllable luminescent single crystal CaF_2 nanocubes. Chem. Commun. (2003). https://doi.org/10.1039/B303614F

22. W. Gong, Z. Fu, S. Zhou, S. Du, S. Zhang, Z. Dai, W. Li, Template-free hydrothermal synthesis and luminescent properties of octahedral $NaGd(MoO_4)_2$:Eu^{3+} microcrystals. J. Electrochem. Soc. **157**, J338–J341 (2010)

23. T. Liu, Q. Meng, W. Sun, Electron-phonon coupling properties and energy transfer in $NaY(WO_4)_2$:Eu^{3+} phosphor. J. Alloys Compd. **647**, 830–836 (2015)

24. A.J. Peter, I.B.S. Banu, Synthesis and luminescence properties of $NaLa(WO_4)_2$:Eu^{3+} phosphors for white LED applications. J. Mater. Sci.: Mater. Electron. **28**, 8023–8028 (2017)

25. X. Liu, L. Li, H.M. Noh, J.H. Jeong, K. Jang, D.S. Shin, Controllable synthesis of uniform $CaMoO_4$:Eu^{3+},M^+(M = Li, Na, K) microspheres and optimum luminescence properties. RSC Adv. **5**, 9441–9454 (2015)

26. W. Ding, P. Liang, Z.H. Liu, Luminescence properties in relation to controllable morphologies of the $InBO_3$:Eu^{3+} phosphor. Mater. Res. Bull. **94**, 31–37 (2017)

27. X. Liu, W. Hou, X. Yang, Q. Shen, Morphology controllable synthesis of $NaLa(WO_4)_2$: the morphology dependent photoluminescent properties and single-phased white light emission of $NaLa(WO_4)_2$: Eu^{3+}/Tb^{3+}/Tm^{3+}. CrystEngComm **16**, 1268–1276 (2013)

28. L. Hou, S. Cui, Z. Fu, Z. Wu, X. Fu, J.H. Jeong, Facile template free synthesis of $KLa(MoO_4)_2$:Eu^{3+},Tb^{3+} microspheres and their multicolor tunable luminescence. Dalton Trans. **43**, 5382–5392 (2014)

29. B.L. Abrams, P.H. Holloway, Role of the surface in luminescent processes. Chem. Rev. **104**, 5783–5801 (2004)

30. A. Durairajan, D. Balaji, K.K. Rasu, S.M. Babu, Y. Hayakawa, M.A. Valente, Sol–gel synthesis and photoluminescence studies on colour tuneable Dy^{3+}/Tm^{3+} co-doped $NaGd(WO_4)_2$ phosphor for white light emission. J. Lumin. **157**, 357–364 (2015)

31. J. Liao, H. You, B. Qiu, H.R. Wen, R. Hong, W. You, Z. Xie, Photoluminescence properties of $NaGd(WO_4)_2$:Eu^{3+} nanocrystalline prepared by hydrothermal method. Curr. Appl. Phys. **11**, 503–507 (2011)

32. F. Estebanbetegón, C. Zaldo, C. Cascales, Hydrothermal Yb^{3+}-doped $NaGd(WO_4)_2$ nano- and micrometer-sized crystals with preserved photoluminescence properties. Chem. Mater. **22**, 2315–2324 (2010)